



**HAL**  
open science

## Automatic detection of fast ripples.

Gwenael Birot, Amar Kachenoura, Laurent Albera, Christian G. Bénar,  
Fabrice Wendling

► **To cite this version:**

Gwenael Birot, Amar Kachenoura, Laurent Albera, Christian G. Bénar, Fabrice Wendling. Automatic detection of fast ripples.. *Journal of Neuroscience Methods*, 2012, 213 (2), pp.236-249. 10.1016/j.jneumeth.2012.12.013 . hal-00782646

**HAL Id: hal-00782646**

**<https://hal.science/hal-00782646>**

Submitted on 30 Jan 2013

**HAL** is a multi-disciplinary open access archive for the deposit and dissemination of scientific research documents, whether they are published or not. The documents may come from teaching and research institutions in France or abroad, or from public or private research centers.

L'archive ouverte pluridisciplinaire **HAL**, est destinée au dépôt et à la diffusion de documents scientifiques de niveau recherche, publiés ou non, émanant des établissements d'enseignement et de recherche français ou étrangers, des laboratoires publics ou privés.

# Automatic detection of fast ripples

**Gwénaél Birot<sup>1,2</sup>, Amar Kachenoura<sup>1,2</sup>, Laurent Albera<sup>1,2</sup>, Christian Bénar<sup>3,4</sup>, Fabrice  
Wendling<sup>1,2</sup>**

<sup>1</sup>INSERM, U1099, Rennes, F-35000, France

<sup>2</sup>Université de Rennes 1, LTSI, F-35000, France

<sup>3</sup>INSERM, U1106, Marseille, F-13000, France

<sup>4</sup>AP-HM, Hôpital de la Timone, Service de Neurophysiologie Clinique, Marseille, F-13000,  
France

Corresponding author: [fabrice.wendling@univ-rennes1.fr](mailto:fabrice.wendling@univ-rennes1.fr)

Published in the Journal of Neuroscience Methods – vol. 213, no. 2, pp. 236-249, March 2013

## 1 **Highlights**

- 2 1) We propose a novel method for automatically detecting fast ripples (FRs, 250-600 Hz)
- 3 2) The signal energy in low and high frequency bands is used to classify EEG events as FRs, interictal  
4 epileptic spikes or artifacts.
- 5 3) The sensitivity and the specificity of this method is high enough to avoid “false ripples” caused by  
6 sharp transients.

## 10 **Abstract**

11 *Objective:* We propose a new method for automatic detection of fast ripples (FRs) which have been  
12 identified as a potential biomarker of epileptogenic processes.

13 *Methods:* This method is based on a two-stage procedure: i) global detection of events of interest  
14 (EOIs, defined as transient signals accompanied with an energy increase in the frequency band of  
15 interest 250-600 Hz), and ii) local energy vs. frequency analysis of detected EOIs for classification as  
16 FRs, interictal epileptic spikes or artifacts. For this second stage, two variants were implemented based  
17 either on Fourier or Wavelet Transform. The method was evaluated on simulated and real depth-EEG  
18 signals (human, animal). The performance criterion was based on receiving operator characteristics.

19 *Results:* The proposed detector showed high performance in terms of sensitivity and specificity.

20 *Conclusions:* As designed to specifically detect FRs, the method outperforms any method simply  
21 based on the detection of energy changes in high-pass filtered signals and avoids spurious detections  
22 caused by sharp transient events often present in raw signals

23 *Significance:* In most of epilepsy surgery units, huge data sets are generated during pre-surgical  
24 evaluation. We think that the proposed detection method can dramatically decrease the workload in  
25 assessing the presence of FRs in intracranial EEGs.

## 28 **Keywords**

29 EEG, epilepsy, fast ripple, interictal epileptic spike, detection, time-frequency, Fourier transform,  
30 wavelet transform, filtering

1 **Glossary**

2 ART: ARTifact

3 AuC: Area under ROC curve

4 EEG: Electro-EncephaloGram or Electro-EncephaloGraphic

5 EOI: Event Of Interest

6 EONI: Event Of Non-Interest

7 FP: False Positive

8 FR: Fast Ripple

9 FRBR: Fast Ripple to Background Ratio

10 FPR: False Positive Ratio

11 FTM: Fourier Transform based Method

12 HFO: High Frequency Oscillation

13 HPFM: High-Pass Filtering Method

14 IES: Interictal Epileptic Spikes

15 ROC: Receiver Operating Characteristic

16 TLE: Temporal Lobe Epilepsy

17 TP: True Positive

18 TPR: True Positive Ratio

19 WTM: Wavelet Transform based Method

20

# 1 Introduction

2 High frequency oscillations (HFOs) have been a topic of increasing interest in neuroscience over the  
3 past decade. They now constitute a novel trend in neurophysiology (Jefferys et al., 2012) that has been  
4 made possible with the development of digital EEG equipments allowing for high sampling rates and  
5 with the identification of oscillations at up to 600 Hz in animals (Buzsaki and Lopes da Silva, 2012).  
6 Among the wide diversity of HFOs which dominant frequency can vary from 30 Hz to 600 Hz, fast  
7 ripples (FRs) are particular transient oscillations (a few tens of ms) occurring in the frequency band  
8 ranging from 250 Hz to 600 Hz. In the normal brain (monkey), FRs have been associated with cortical  
9 spike bursts (Baker et al., 2003). In the epileptic brain, FRs were shown to be related to abnormal  
10 modifications in the excitability of underlying neuronal systems (Demont-Guignard et al., 2012).  
11 Epileptic FRs have first been observed in animal models (Bragin et al., 1999b) as well as in patients  
12 with drug-resistant partial epilepsy (Bragin et al., 1999a). A number of studies then confirmed the  
13 existence of interictal HFOs in brain structures involved at the onset of seizures (Bragin et al., 2002;  
14 Jacobs et al., 2008; Worrell et al., 2004) and the potential value of FRs as a marker of the degree of  
15 epileptogenicity (Engel et al., 2009; Jacobs et al., 2009; Worrell and Gotman, 2011).

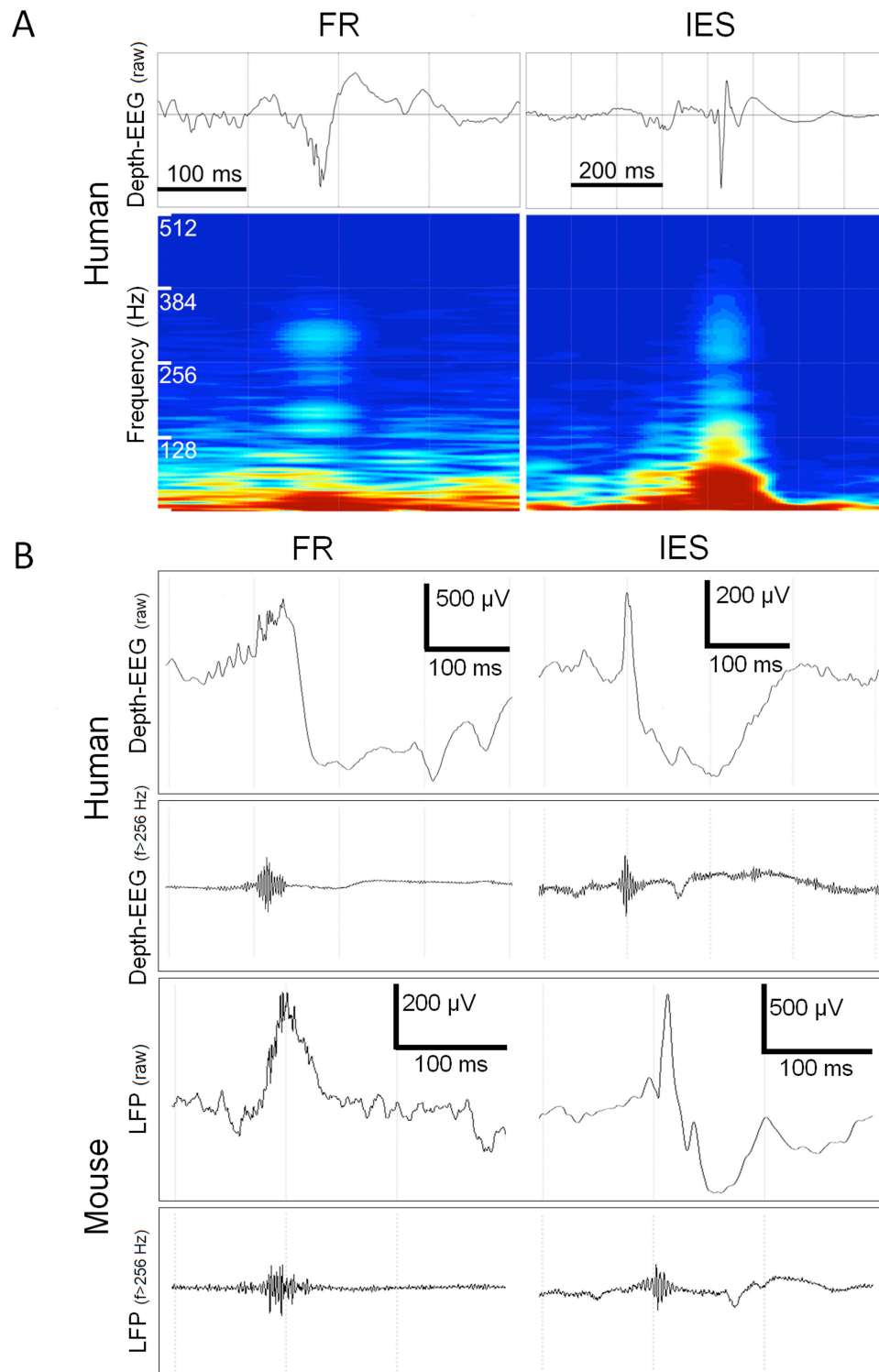
16 In this context, the accurate detection of FRs in depth-EEG signals recorded in patients candidate to  
17 surgery could considerably improve the identification and delineation of the epileptogenic zone which  
18 is an essential step in planning the best therapeutic strategy (Bartolomei et al., 2002). However, this  
19 detection is far from being a trivial problem. In most of aforementioned studies, the detection of FRs  
20 was performed visually by inspecting either the raw signals or the filtered signals in the frequency  
21 band of interest (beyond 80 Hz). However, on the one hand, the visual inspection of EEG signals  
22 remains fastidious. Indeed, the number of events of interest (EOIs) occurring during interictal periods  
23 can be potentially high. In addition, the review of EEGs must be performed with an appropriate time  
24 scale (strongly magnified w.r.t. those classically used) in order to visually assess the actual presence  
25 (or absence) of transient oscillations associated with EOIs. The detection of FRs can also be helped by  
26 the use of simple signal processing algorithms like, in particular, the filtering of depth-EEG signals in  
27 the frequency band of interest (typically beyond 250 Hz). However, on the other hand, as shown in

1 (Benar et al., 2010), any high-pass filtering technique has one major pitfall: the lack of specificity due  
2 to sharp transients present in depth-EEG signals. Indeed, in this study, authors could verify that some  
3 “pulse-like” events (typically, the spike component of interictal epileptic spikes - IES) are associated  
4 with an abrupt increase of the signal energy in the higher frequency bands, exactly as in the case of  
5 actual FRs. A typical example is provided in Figure 1A. As a consequence, the oscillations generated  
6 in the filtered signal that are related to the features of the impulse response of the high-pass filter can  
7 be confounded with actual FRs, leading the authors to denote them as “false ripples” (Figure 1B).

8 In this context, the demand is high for automatic detection procedures with increased specificity, while  
9 maintaining a good sensitivity. In this paper, we propose a novel detection method for automatically  
10 identifying FRs occurring in depth-EEG signals. To our knowledge, very few methods have been  
11 proposed so far to achieve this goal. A few years ago, band-pass filtering techniques were combined  
12 with a thresholding procedure of the energy of sub-band signals to automatically detect HFOs (Crepon  
13 et al., 2010; Gardner et al., 2007; Staba et al., 2002). Very recently, Zelman and colleagues (Zelmann  
14 et al., 2012) proposed a new method (referred to as the MNI detector) and compared it to the three  
15 aforementioned ones. The initial step of their method was also based on a band-pass filter (80-450 Hz)  
16 but included a baseline analysis (based on wavelet entropy) to differentiate channels with transient  
17 HFOs from those with continuous HF activity. The decision (presence/absence of a HFO) was based  
18 on a threshold. While these methods offer a good sensibility they exhibit poor specificity due to sharp  
19 IES or artifacts often present in raw signals. The method proposed in (Blanco et al., 2010) makes use  
20 of the result of the Staba’s method as a first step and then automatically classifies the resulting  
21 candidate events using a data mining algorithm. The method could separate actual HFOs (including  
22 ripples and FRs) from artifacts in a very large data set but the issue of spurious detections due to IES  
23 was not addressed.

24 In contrast, our detection method was designed to exclusively recognize FRs and to avoid false  
25 detections caused by sharp transient events (typically IES). It is based on a two-stage procedure: i)  
26 global detection of EOIs, defined as transient signals accompanied with an energy increase in the  
27 frequency band of interest (250-600 Hz) and ii) local energy vs. frequency analysis of detected EOIs

1 for classification as FRs, IESs or artifacts. For this second stage of the detection procedure, two



2

3 **Figure 1:** Typical FRs and IESs recorded from hippocampus in human (TLE) and in an animal model of epilepsy

4 (mouse, kainate model). (A) Human FRs and IESs (depth-EEG signals) with corresponding spectrograms. Note

5 that both EOIs (the FR and the IES) exhibit energy in the 250-600 Hz. (B) FRs and IESs recorded from

6 hippocampus using macro-electrodes (human: depth-EEG, mouse: LFPs). Upper plots: raw signals. Lower plots:

1 filtered signals (high-pass cutoff frequency = 256 Hz). Note that the two types of epileptic events can hardly be  
 2 discriminated using a simple high-pass filtering procedure.

3

4 variants were implemented based either on Fourier or Wavelet Transform. Performance was first  
 5 evaluated on real depth-EEG data recorded in human (temporal lobe epilepsy - TLE) as well as in an  
 6 experimental in vivo model of TLE (mouse kainate). It was also evaluated on simulated signals which  
 7 consisted of real FRs and IESs (assessed by the expert) inserted at known occurrence times in an EEG  
 8 background activity generated with a realistic computational model of hippocampal activity  
 9 (Wendling et al., 2005). We also provided how to calculate the optimal threshold that allows the  
 10 discrimination of FRs from IESs in the method. Results showed that the proposed detection method  
 11 can achieve good performance with relatively few parameters to adjust. As an important finding, best  
 12 results were obtained when the energy ratio between oscillations in the FR band vs. gamma band was  
 13 used as a discriminant factor in the second stage of the detection procedure.

## 14 **2 Material and methods**

### 15 **2.1 Problem formulation and notations**

16 The depth-EEG signal on which the detection is performed is denoted by  $\{s[n]\}$ . This signal mainly  
 17 contains background (denoted by  $\{BKG[n]\}$ ) activity in which some transient events may appear  
 18 randomly. These transient events include i) events of interest (EOIs) characterized by significant  
 19 energy (compared to BKG) in the frequency band of interest, typically ranging from 250-600 Hz  
 20 (rounded to 256-512 Hz in our case for methodological reason) and ii) some other events of non-  
 21 interest (EONI) exhibiting energy at lower frequencies. The occurrence time of the  $p$ th EOI is denoted  
 22 by  $t_p$ . Each EOI is assumed to have a finite time support of length less than  $2K$  (values used in practice  
 23 are discussed in section 2.5). Thus the  $p$ th EOI's time support in  $\{s[n]\}$  is delimited by  
 24  $\{t_p - K, K, t_p, K, t_p + K - 1\}$ . Consequently the depth-EEG signal at time  $n$  can be written as

$$25 \quad s[n] = BKG[n] + \sum_{p=1}^P EOI_p[n - t_p] + EONI[n]$$

1 where  $\{\text{EOI}_p[n]\}$  denotes the time course of the  $p$ th EOI,  $t_p$  is the time instant where it occurs,  $P$  is  
 2 the number of EOIs and  $\{\text{EONI}[n]\}$  is the time course of other transient events (of non-interest). The  
 3 EOIs are classified in three types: fast ripples (FRs), interictal epileptic spikes (IESs) and artifacts.  
 4 Accordingly, the depth-EEG signal can be expressed as

$$5 \quad s[n] = \text{BKG}[n] + \sum_{p=1}^{P_{\text{FR}}} \text{FR}_p[n - t_p^{\text{FR}}] + \sum_{p=1}^{P_{\text{IES}}} \text{IES}_p[n - t_p^{\text{IES}}] + \sum_{p=1}^{P_{\text{ART}}} \text{ART}_p[n - t_p^{\text{ART}}] + \text{EONI}[n]$$

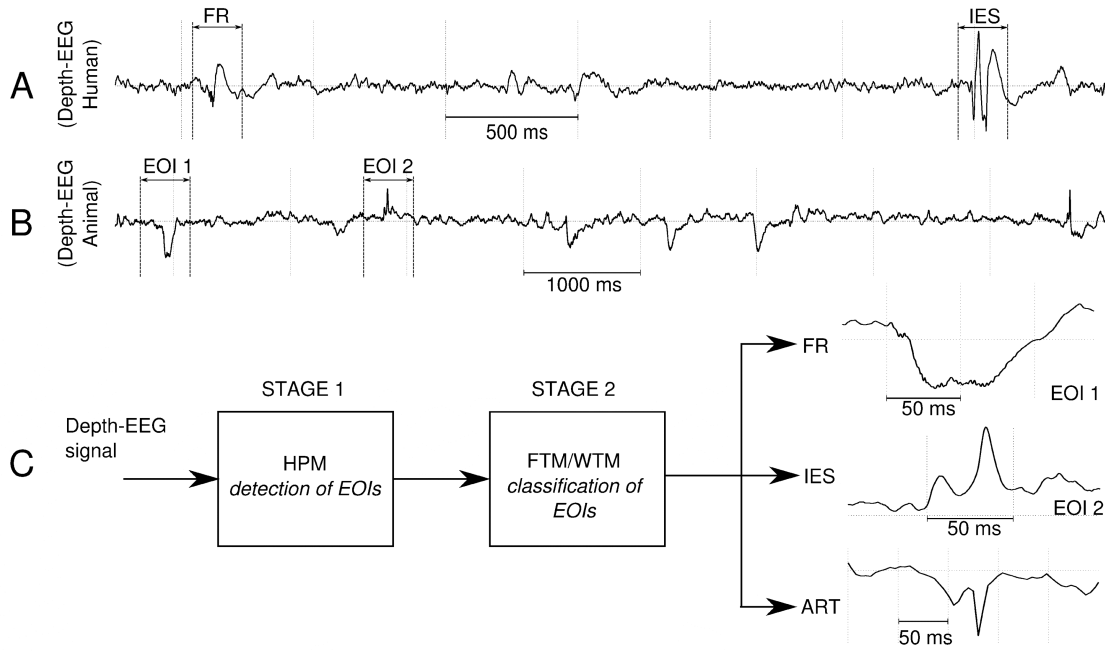
6 where  $\text{FR}_p[n]$ ,  $\text{IES}_p[n]$  and  $\text{ART}_p[n]$  are the time course of the  $p$ th FR, IES and artifact,  
 7 respectively,  $t_p^{\text{FR}}$ ,  $t_p^{\text{IES}}$  and  $t_p^{\text{ART}}$  are the times where they occur, respectively, and  $P^{\text{FR}}$ ,  $P^{\text{IES}}$  and  
 8  $P^{\text{ART}}$  are the number of FRs, IESs and artifacts, respectively.

9 The proposed methods aim at detecting the occurrence times of FR, i.e.  $t_p^{\text{FR}}$  for  $p$  varying from one to  
 10  $P^{\text{FR}}$ .

## 11 **2.2 Proposed detection methods**

### 12 **2.2.1 Basic principle**

13 Our FR detector involves two stages (figure 2). In the first stage, events of potential of interest (EOIs =  
 14 events exhibiting significant energy in the frequency band greater than 256 Hz, among which IESs,  
 15 FRs and artifacts) are detected. This is done using a simple method based on high-pass filtering  
 16 (HPFM), as depicted in figure 3A. We used here a very simple method but all HFO detectors based on  
 17 high-pass filtering could work (e.g. method given by (Staba et al., 2002)). Then, the second stage  
 18 consists in the recognition of FRs among detected EOIs. This step is the most important and is the  
 19 main contribution of our work. We tested two methods both based on the ratio between the energy in  
 20 high frequency band and the energy in low frequency band (see Figures 2B and 2C). The first method,  
 21 called Fourier Transform based Method (FPM) uses a short-term Fourier Transform while the second  
 22 method, called Wavelet Transform based Method (WTM), uses multi-resolution discrete Wavelet  
 23 Transform.



1  
2 **Figure 2:** Overview of the method for automatic detection of FRs. The human depth-EEG signal (A) and animal  
3 depth-EEG signal (B) exhibits FRs and IESs. With a simple high-pass filter, very sharp components of the IESs  
4 could be interpreted as a FRs. In the proposed methodology (C), stage 1 (HPFM) allows for the detection of  
5 events (FRs, IESs and some artifacts) exhibiting significant energy in the FR band (256-512 Hz). The second  
6 stage acts as a classifier and separates FRs from the other EOIs. This classification is achieved using the energy  
7 ratio between the HF (256-512 Hz) band and lower frequency band. The energy ratio is computed using either a  
8 short-time Fourier Transform (FTM) or a dyadic wavelet transform (WTM). See glossary for abbreviations.

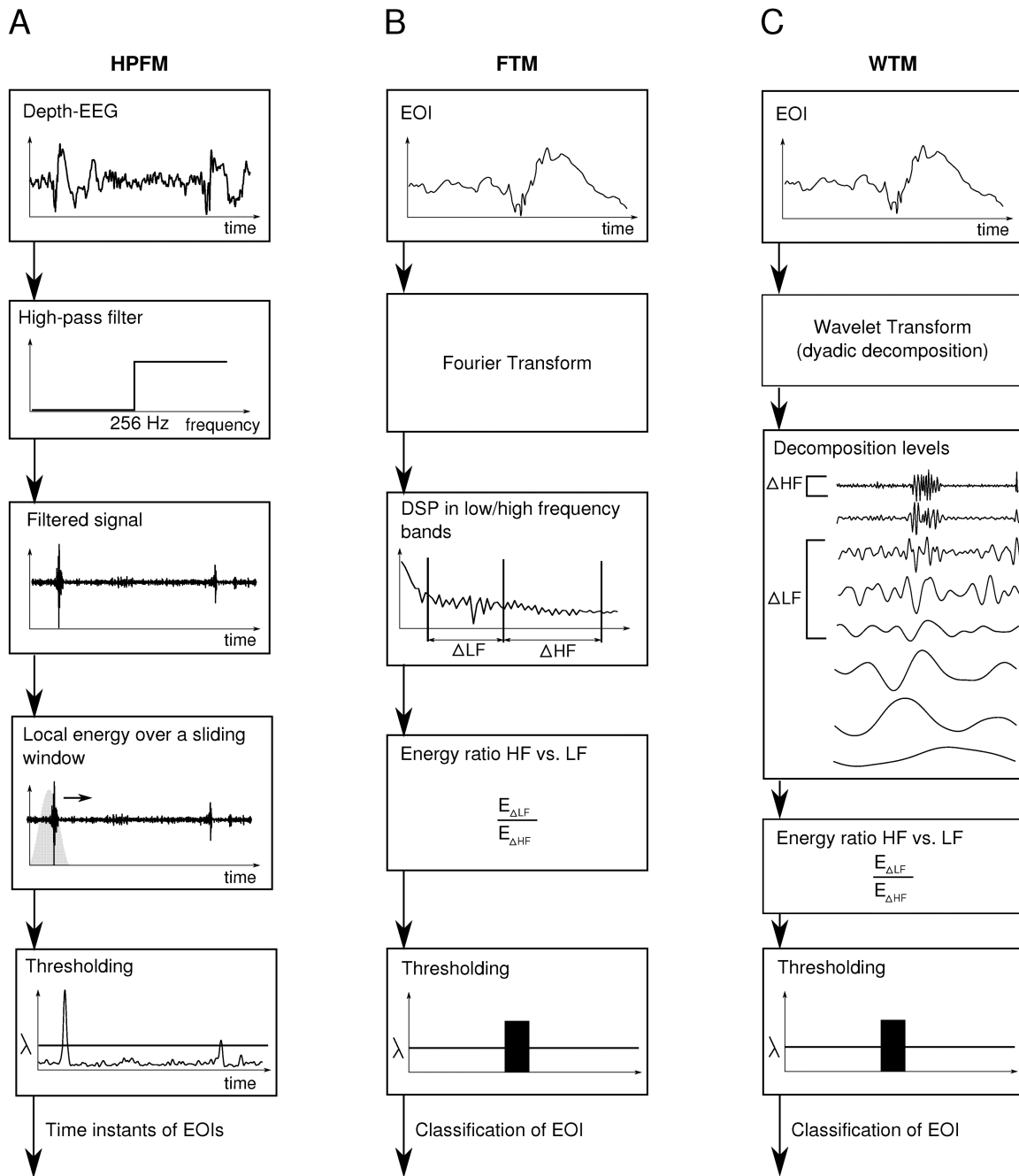
9

## 10 2.2.2 Stage 1: detection of EOIs (HPFM)

11 The detection of EOIs was performed with high-pass filtering of cut-off frequency equal to 256 Hz.  
12 An IIR high-pass filter of order  $O$  was used (Butterworth,  $O=4$ , 80 dB/decade). The filtered signal at  
13 time  $n$  is given by:

$$14 s_{\text{hp256}}[n] = \frac{1}{a_0} \left( \sum_{i=0}^O b_i s[n-i] - \sum_{j=1}^O a_j s_{\text{hp256}}[n-j] \right)$$

15 where  $a_j$  and  $b_i$  are the coefficient of the filter. By definition, in this filtered signal  $s_{\text{hp256}}[n]$  the  
16 contribution of  $\{\text{EONI}[n]\}$  is vanished while a significant contribution of EOIs is preserved.



1  
2 **Figure 3:** Step-by-step pipeline of studied methods (HPFM, FTM and WTM). (A) HPFM consists in i) high-pass  
3 filtering the signal (cut-off frequency = 256 Hz), ii) calculating the short-time energy of the filtered signal and iii)  
4 finding the local maxima of the short-time energy greater than a threshold in order to estimate the occurrence  
5 times of EOIs. (B) FTM consists in computing the short-time Fourier transform at the instant of detected EOIs, ii)  
6 calculating the ratio between the EOI energy in the HF band vs. in the LF band, and iii) thresholding this ratio in  
7 order to separate FRs from IESs and artifacts. (C) WTM consists in i) computing the dyadic wavelet transform of  
8 the EOI, ii) calculating the ratio between energy of the decomposition level corresponding to the 256-512 Hz and  
9 decomposition levels of lower frequencies and iii) thresholding this ratio in order to identify FRs. See glossary for  
10 abbreviations.

1 A contribution of the background activity (BKG) may also be present since rest depth-EEG signals  
 2 have a wide frequency spectrum, including frequencies greater than 256 Hz. Thus, the filtered signal at  
 3 time  $n$  can be expressed as:

$$4 \quad s_{\text{hp}256}[n] = \text{hp}(\text{BKG}[n]) + \sum_{p=1}^P \text{hp}(\text{EOI}_p[n - t_p])$$

5  
 6 where  $\text{hp}(\cdot)$  is the high pass filter function. Assuming that the level of BKG in the 256-512 Hz band is  
 7 not higher than the level of EOIs in the 256-512 Hz band, the local maxima of the local energy of  
 8  $s_{\text{hp}256}[n]$  correspond to the occurrence times of EOIs.

9 The local energy  $\{E_{\text{hp}256}[t]\}$  of the filtered signal can be calculated using a sliding Hanning window  
 10 of duration  $N$  denoted by  $\{h_N[n]\}$ . Therefore, we have:

$$11 \quad E_{\text{hp}256}[t] = \sum_{n=-\infty}^{\infty} (s_{\text{hp}256}[n])^2 h_N[n - t] \quad (1)$$

12 Estimated occurrence times of EOIs,  $\hat{t}_p$ , are eventually computed as the arguments of the local  
 13 maxima of  $E_{\text{hp}256}[t]$  greater than a threshold  $\beta$ :

$$14 \quad \{\hat{t}_1(\beta), \dots, \hat{t}_p(\beta)\} = \left\{ \arg \max_t (E_{\text{hp}256}[t]), E_{\text{hp}256}[t] > \beta \right\}$$

15 where the  $\arg \max$  function stands for the search of local maxima. In practice, threshold  $\beta$  is adjusted  
 16 from the distribution of  $E_{\text{hp}256}$ . Typically, in this study, we chose  $\beta$  for any  $t$  value such that the  
 17 probability that  $E_{\text{hp}256}[t] < \beta$  is greater than 0.98 (i.e. 98 percentile) for both simulated and real data.

### 18 **2.2.3 Stage 2: Classification of EOI's (FTM and WTM)**

19 As mentioned, the goal of the EOI classifier is to extract fast ripples from other events detected at the  
 20 first step, especially IESs. We introduce two methods to achieve this extraction, both based on the  
 21 ratio between the energy in the high frequency (HF) band and in the low frequency (LF) band.

22 *Method 1: Fourier Transform based Method (FTM)*

1 The first proposed method is based on the digital short-time Fourier transform (with rectangular  
2 window) at time  $t_p$  of the depth-EEG signal  $\{s[n]\}$ :

$$3 \quad S(f, t_p) = \sum_{n=t_p-K}^{t_p+K-1} s[n] e^{-2i\pi f \frac{n}{2K}}$$

4 The energy in a specific frequency band  $\Delta f = \{f_1, K, f_K\}$  of the  $p$ th EOI is thus given by:

$$5 \quad E_{\Delta f}(p) = \sum_{f \in \Delta f} |S(f, t_p)|^2$$

6 The criterion we propose to identify FRs is based on an energy ratio. First, we compute the energy of  
7 EOIs in the high frequency band  $\Delta_{HF}$  ( $f \geq 256$  Hz) and in the low frequency band  $\Delta_{LF}$ . The energies

8 of the  $p$ th EOI in the HF and LF bands are given by  $E_{\Delta HF}(p)$  and  $E_{\Delta LF}(p)$ , respectively. Then, the

9 decision is made on  $E_{\Delta HF/LF}^{FTM}(p) = E_{\Delta HF}(p) / E_{\Delta LF}(p)$ . The estimated indices  $\hat{p}_{FR}^{FTM}$  of EOIs

10 corresponding to FRs are such that the ratio  $E_{\Delta HF/LF}^{FTM}(p)$  is greater than a threshold  $\lambda_1$  (see section 2.5

11 for practical value):

$$12 \quad \{\hat{p}_{FR}^{FTM}(\lambda_1)\} = \{p, E_{\Delta HF/LF}^{FTM}(p) > \lambda_1\} \quad (2)$$

13 In practice, it is noteworthy that the LF band was let as a free parameter (optimized from results, see  
14 section 3) while the HF band was fixed to 256-512 Hz.

15 *Method 2: Wavelet Transform based Method (WTM)*

16 The second proposed method is based on the ratio between energy in different levels of a dyadic  
17 wavelet transform of the EOIs. The dyadic wavelet transform of the depth-EEG signal  $\{s[n]\}$  over the

18  $p$ th EOI of time support  $\{t_p - K, K, t_p, K, t_p + K - 1\}$  can be written as:

$$19 \quad W_p(2^j, t) = \sum_{n=t_p-K}^{t_p+K-1} s[n] 2^{j/2} \psi[2^j n - t]$$

20 where  $j$  is the decomposition level and  $\psi$  is the mother wavelet. The level  $j$  of the dyadic

21 decomposition contains the contribution of the signal including frequencies between  $f_s/2^j$  and  $f_s/2^{j+1}$

22 where  $f_s$  is the sampling frequency. The energy at level  $j$  of the wavelet decomposition of the  $p$ th EOI

23 is given by the sum over time of the square wavelet transform:

$$E^{(j)}(p) = \sum_t (W_p(2^j, t))^2$$

As for the above-described FTM, the criterion that allows for the classification of the  $p$ th EOI is given by the ratio between energy in HF levels and LF levels:

$$E_{\Delta_{\text{HF/LF}}}^{\text{WTM}}(p) = \frac{\sum_{j \in \Delta_{\text{HF}}} E^{(j)}(p)}{\sum_{j \in \Delta_{\text{LF}}} E^{(j)}(p)}$$

In practice, the set of levels  $j \in \Delta_{\text{HF}}$  included only one level ( $j = 1$  at  $f_s = 1024$  Hz or  $j = 2$  at  $f_s = 2048$  Hz) corresponding to the 256-512 Hz frequency band while the set  $j \in \Delta_{\text{LF}}$  corresponding to low frequencies was also let a free parameter (the influence of which is analysed in section 3). Eventually, the occurrence times of EOIs that correspond to FRs are estimated for a given threshold  $\lambda_2$  by:

$$\{\hat{p}_{\text{FR}}^{\text{WTM}}(\lambda_2)\} = \{p, E_{\Delta_{\text{HF/LF}}}^{\text{WTM}}(p) > \lambda_2\} \quad (3)$$

10  
11

## 2.3 Real and simulated signals

### 2.3.1 Human data

Intracerebral stereo-EEG (SEEG or depth-EEG) signals were used for the purpose of this study. Signals were recorded in patients ( $n=2$ ) suffering from mesial TLE. The depth-EEG exploration was carried out as part of normal clinical care of both patients. Informed consent was given by patients about the use of data for research purposes. Only signals recorded from electrode contacts located in the hippocampus (Ammon's horn) were used as many FRs as well as IESs could be observed in this brain structure (Figure 2A). Intracerebral electrodes are composed of 10 to 15 cylindrical contacts (length: 2 mm, diameter: 0.8 mm, 1.5 mm apart). Two contacts (more mesial) are usually located in the hippocampus. For the purpose of this study, we chose the electrode contact at which the highest number of EOIs was observed. About 300 EOIs were visually detected in several hours of recording and annotated as FRs (about 150) or IESs (about 150) by the expert (see Table 1). The visual

1 annotation was helped by the use of an EEG review software (Amadeus, developed in the lab - LTSI,  
2 University of Rennes -) allowing for strong magnification of the time-scale (1 sec/page). It is worth  
3 mentioning that visually detected events were quite representative of those recorded from the  
4 hippocampus in mesial TLE according to our experience. Regarding the behavioral state of the two  
5 patients, visual analysis of the videos corresponding to analyzed periods of depth-EEG data showed  
6 that both patients were lying on the bed. They were awake. Eyes were opened. Both patients were  
7 interacting with some other people present in the room. Signals were recorded on a 128-channel  
8 Micromed™ system and were sampled at  $f_s=1024$  Hz. No hardware filter was present in the  
9 acquisition procedure except the high-pass filter (cut-off frequency about 0.1 Hz) classically used to  
10 remove the offset on the baseline. The 3D position of the electrode exploring the anterior hippocampus  
11 was anatomically checked from the fusion of the telemetric X-ray imaging performed per-operatively  
12 (on which the electrode contacts are clearly visible) and the post-operative MRI scan (on which the  
13 trajectory of each electrode remains visible).

### 14 **2.3.2 Animal data**

15 Depth-EEG signals recorded in freely moving mice ( $n=4$ ) treated with kainic acid (KA) were also used  
16 for this study. Readers may refer to (Suzuki et al., 1995) for details about this kainate model of TLE.  
17 In brief, it was shown to closely replicate some pathological changes observed in human mTLE. These  
18 changes include both histological alterations and interictal/ictal electrophysiological patterns. The  
19 model is based on a unilateral injection of a low dose of KA into the dorsal hippocampus of mice.  
20 After injection, mice were implanted with bipolar depth electrodes (consisting of two twisted polyester  
21 insulated stainless steel wires, 139  $\mu\text{m}$  diameter each and 0.3 mm apart) in both hippocampi (CA1  
22 region). After a latent period of about 2 weeks, spontaneous seizures begin to occur, accompanied by a  
23 progressive cell loss in the CA1 and CA3 regions of the hippocampus over a period of 4 to 6 weeks  
24 (Bouilleret et al., 2000; Suzuki et al., 1995). Upon completion of the experiments, histological  
25 analyses were performed to verify the location of the KA injection, the location of the hippocampal  
26 electrode and the pattern of neuronal loss/dispersion of dentate gyrus granule cells. All animal

1 procedures were conducted in accordance with the European Communities Council Directive of 24  
 2 November 1986 (86/609/EEC). The experimental design was made to minimize animal suffering.

3

<b>Data set</b>	<b>Duration (s)</b>	<b>Recorded brain structure</b>	<b>Number of FRs</b>	<b>Number of IES</b>
<b>human #1</b>	4000	Anterior hippocampus	62	95
<b>human #2</b>	2000	Posterior hippocampus	80	61
<b>mouse #1</b>	7200	Hippocampus (CA1), ipsilateral to KA injection	318	50
<b>mouse #2</b>	1500	Hippocampus (CA1) contralateral to KA injection	75	161
<b>mouse #3</b>	7200	Hippocampus (CA1) contralateral to KA injection	0	182
<b>mouse #4</b>	914	Hippocampus (CA1), ipsilateral to KA injection	680	0

4

5 **Table 1:** Details about the recordings used in this study.

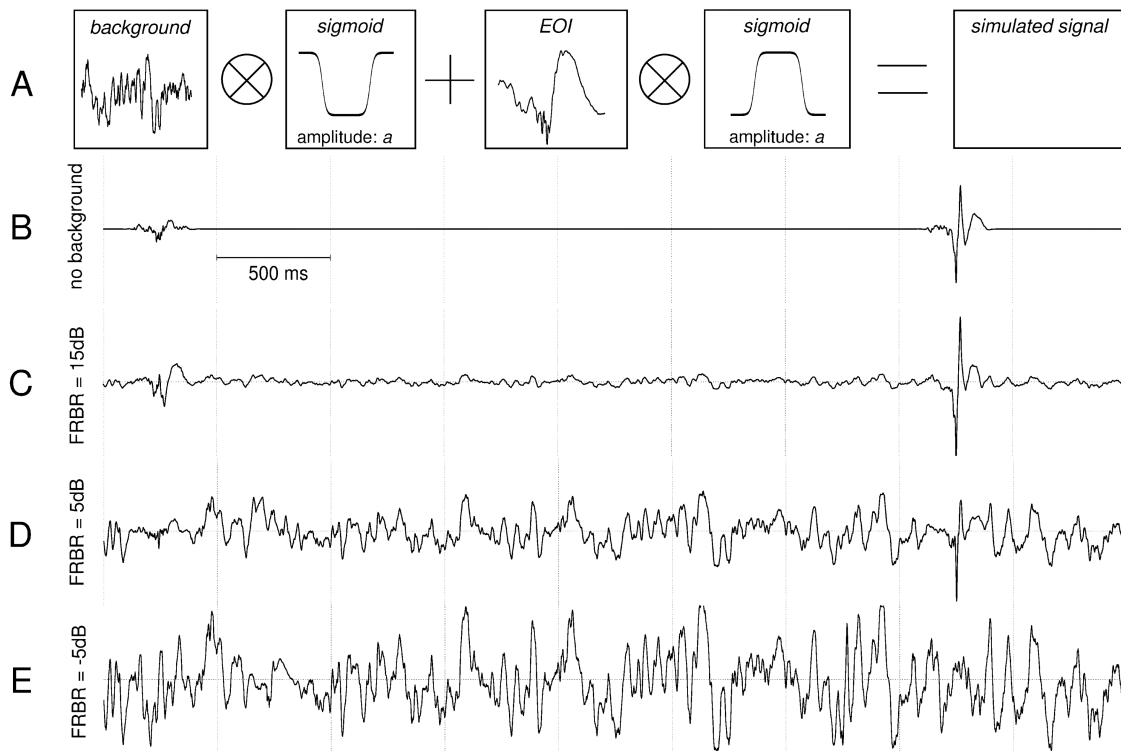
6

7 Depth-EEG signals were recorded on a video-EEG monitoring system (Deltamed TM). They were  
 8 sampled at  $f_s=2048$  Hz. One hardware high-pass filter was present in the acquisition procedure (cut-off  
 9 frequency: 0.16 Hz). It has no effect on the shape of EOIs. A key point of this experimental model is  
 10 that during the latent period and the chronic period, both IESs and FRs are frequently observed in  
 11 depth-EEG signals, as show in Figure 2B. As for human data, the review of depth-EEG signals and the  
 12 annotation of EOIs (about 400 IESs and 1000 FRs, see Table 1) was assessed by the same expert who  
 13 used the aforementioned EEG review software allowing for magnification of the time scale.

### 14 **2.3.3 Simulated signals**

15 In order to assess the detector performance with respect to the level of background activity, simulated  
 16 long-duration signals in which transient events extracted from the real data (see subsections 2.3.1 and  
 17 2.3.2) were mixed up with simulated EEG background activity. This background activity was  
 18 generated using a realistic model of neuronal population described elsewhere (Wendling et al., 2005).

1

2  
3

**Figure 4:** Generation of simulated depth-EEG signals. (A) EOIs extracted from real data were inserted in simulated background activity. The background level was controlled and quantified by the fast ripple to background ratio (FRBR). Examples of simulated depth-EEG including one FR and one IES for FRBR =  $\infty$  (B), FRBR = 15 dB (C), FRBR = 5 dB (D), FRBR = -5 dB (E). See glossary for abbreviations.

6  
7

8 The extracted segments of real data that contained the transient events had a length of 512 ms. In order  
9 to avoid any discontinuity in the generated signal (potentially leading to unwanted sharp transients), a  
10 weighting function (sigmoid shape) was used to obtain a smooth transition at the junction between the  
11 inserted event and the background activity (see Figure 4A). The transient events appeared randomly in  
12 the simulated signal following a Poisson's law allowing us to set the mean number of occurrence of  
13 each type of transient events per minute. The level of background activity was controlled by a  
14 multiplicative coefficient and was quantified by the Fast Ripple to Background Ratio (FRBR). The  
15 FRBR quantity was defined as the mean power of FRs relative to the mean power of background  
16 activity:

$$1 \quad \text{FRBR} = 10 \log \left[ \frac{\frac{1}{\text{card}(\Delta_{\text{FR}})} \sum_{n \in \Delta_{\text{FR}}} (s[n])^2}{\frac{1}{\text{card}(\Delta_{\text{BKG}})} \sum_{n \in \Delta_{\text{BKG}}} (s[n])^2} \right]$$

2 where  $\Delta_{\text{FR}}$  is the time range where fast ripples occur while  $\Delta_{\text{BKG}}$  is the time range of background  
3 activity. The function  $\text{card}(\cdot)$  gives the cardinal of a range. For each FRBR (-5 dB to  $+\infty$ ), a 60 min  
4 duration signal was simulated with, on average, 8 occurrences of a randomly-chosen EOI per min.  
5 Examples are provided in Figure 3 showing a short segment of simulated signal including a fast ripple  
6 (at time  $t = 0.25$  s) and an interictal spike (at time  $t = 3.75$  s). For high FRBR values (Figure 4B and  
7 4C), both EOIs are clearly visible while they can hardly be distinguished from background as the  
8 FRBR gets lower (Figure 4D and 4E). This is especially true at FRBR = -5 dB (Figure 4E) where both  
9 EOIs become impossible to see.

## 10 **2.5 Performance evaluation**

### 11 **2.5.1 Performance criterion**

12 Studied methods were designed to detect the occurrence times of FRs. According to the signal  
13 detection theory, receiver operating characteristic (ROC) curves were used to quantitatively analyse  
14 the performance of the methods. The ROC curve is a parametric graphical plot representing the True  
15 Positive Rate (TPR, also referred to as “sensitivity”) as a function of the False Positive Rate (FPR,  
16 also referred to as “one minus specificity” or “false alarm rate”). Both values depend on one parameter  
17 that is threshold  $\beta$  for HPFM, threshold  $\lambda_1$  for FTM and threshold  $\lambda_2$  for WTM. Each threshold value  
18 provides a TPR/FPR couple. The complete ROC curves are obtained by varying the threshold value  
19 over a given range.

20 As a complete ROC curve is not handy to show results, we will rather provide the Area under the ROC  
21 Curve (AuC), which corresponds to the integral of the ROC curve for FPR ranging from 0 to 1. The  
22 AuC value ranges between 0.5 (worst result) and 1 (best results) and provides a compact and direct  
23 way of showing method accuracy. Indeed, the perfect detector would exhibit a TPR equal to one for a  
24 FPR equal to zero. In such a case the AuC is equal to one. The worst detector would show a line of

1 slope equal to 1, hence the AuC would be 0.5. In practice the AuC could be slightly less than 0.5 due  
 2 to the variance of the TPF and FPF estimators.

### 3 **2.5.2 Parameters of evaluated methods**

4 The proposed methods depend on explicit parameters. In this section, we provide some parameters we  
 5 used. We chose them with preliminary studies not shown in this paper.

6 For the first step of the procedure (*HPFM*) we used a fourth order IIR Butterworth high-pass filter (80  
 7 dB/decade), which is a good trade-off between performance, stability and complexity. The coefficients  
 8 of this filter were adjusted such that the cut-off frequency was equal to 256 Hz (i.e. the attenuation at  
 9 256 Hz is 3dB). This frequency is in accordance with the FR band. In order to calculate the local  
 10 energy of the filtered signal (eq. 1), we used a Hanning window of  $f_s/8+1$  samples (i.e. 125 ms) which  
 11 we believe is the very maximum duration of FRs.

12 For *FTM*, the duration of EOIs on which the Fourier Transform is calculated was fixed at  $f_s/8$  (250  
 13 ms). The high frequency band was set to be 256-512 Hz in order to maximize the FR energy while the  
 14 low frequency band was let as a free parameter. An analysis of the method performance with respect  
 15 to nine different LF bands was performed (see §2.5.3).

16 For *WTM* the time segment of EOIs was also set to  $f_s/8$  samples (125 ms). From preliminary analysis  
 17 in which we tested several mother wavelets (Daubechies 1 to 10), we used a Daubechies 4 mother  
 18 wavelet. The number of decomposition levels  $N_L$  depended on the sampling frequency. For signals  
 19 sampled at 1024 Hz (human data),  $N_L$  was equal to 8. We retained the first level ( $j=1$ ) as the HF band  
 20 (256-512 Hz). For signals sampled at 2048 Hz (animal data),  $N_L$  was equal to 9. We picked up the  
 21 second level ( $j=2$ ) for the HF band (256-512 Hz). As previously, the levels corresponding to the LF  
 22 band were also let as free parameters for subsequent optimization (see §2.5.3).

### 23 **2.5.3 Optimization of parameter LF in FTM and WTM**

24 In order to determine the optimal LF bands for both FTM and WTM (see eq. 2 and eq. 3), we analysed  
 25 the method performance for nine different values of the LF band: [0,512], [0,256], [0,128], [0,64],  
 26 [0,32], [128,256], [64,128], [32,64] and [32,128] Hz. The optimization was performed using the

1 database of FRs and IES extracted from human and animal data. We determined which low frequency  
2 band (for FTM) and which levels (for WTM) of the wavelet decomposition maximized the Area under  
3 the ROC curve (note that parameter LF does not intervene in HPFM).

#### 4 **2.5.4 Parameters of simulated signals**

5 Simulated signal are determined by three parameters: the occurrence frequency of FRs, the occurrence  
6 frequency of IESs and the level of the background activity. We expected that the occurrence frequency  
7 of transient events has no influence on the performance of the proposed methods. We arbitrarily fixed  
8 this parameter to 4 occurrences per minute for each type of events. Conversely, the level of  
9 background activity was expected to have a significant influence on the algorithm performance, hence  
10 a study of performance with respect to the Fast Ripple to Background Ration (FRBR) was also  
11 performed. To proceed, we used simulated signals when the FRBR was respectively set to infinity (no  
12 background activity), 15dB, 5 dB and -5dB. In addition to FTM and WTM, we also included HPFM in  
13 this study.

#### 14 **2.5.5 Analysis of FTM ( $\lambda_1$ ) and WTM ( $\lambda_2$ ) thresholds**

15 In order to determine the optimal thresholds that best separates FRs from IESs at the second stage of  
16 the algorithm ( $\lambda_1$  for FTM or  $\lambda_2$  for WTM) and the resulting good classification rate, we assumed that  
17 the probability density function of the FTM and WTM criteria for FRs and IESs were Gaussian. Note  
18 that this hypothesis was validated using the Kolmogorov test (Papoulis, 1991). Knowing the analytical  
19 expression of these Gaussian probability density functions, we were able to determine the theoretical  
20 thresholds  $\lambda_1$  and  $\lambda_2$  that maximize the probability of good classification of the EOIs (see details in  
21 appendix A). These optimal thresholds as well as the resulting classification rates depend on the  
22 estimated probability density functions (i.e. the mean and standard deviation of the HF/LF ratio) but  
23 also on the occurrence rate of FRs in the EOIs (i.e. the percentage rate of FRs among the EOIs selected  
24 at first stage). While we believe that the estimated mean and standard deviation are consistent and  
25 reproducible, the occurrence rate of FRs in the EOIs is strongly data dependent. Therefore we first  
26 estimated the optimal threshold as a function of FR rate. Then we calculated the corresponding good

1 classification rate for two different situations: i) the FR rate is known, i.e. we calculated the good  
2 classification rate using optimal threshold computed at appropriate FR rate, ii) the FR rate is unknown,  
3 i.e. we calculated the good classification rate using optimal threshold computed for an arbitrary FR  
4 rate equal to 0.5. The second technique allowed us to know the supplementary errors committed when  
5 FR rate is not known and set to an arbitrary value.

### 6 **3 Results**

7 *Choice of the LF band in methods FTM & WTM.* We performed a sensitivity analysis with respect to  
8 the choice of the LF band for FTM and WTM (2<sup>nd</sup> stage of the proposed detection method). For both  
9 algorithms, the objective was to find which LF band maximizes the separation between FRs and IESs  
10 in EOIs manually selected by the expert. The study was performed both on human and animal data  
11 (data described in § 2.3.1 and 2.3.2). The results for the nine selected frequency bands are reported in  
12 table 3 for human data and in table 4 for animal data. First, for both types of data, results revealed that  
13 both methods showed dependency on this parameter. This was particularly true for FTM. For instance,  
14 in human data (table 3), the TPR at fixed FPR = 0.05 was found to vary from 0.238 (LF = ]128, 256]  
15 Hz) to 0.968 (LF = ]32, 128] Hz). The same result also held for mouse data. Second, the performance  
16 of FTM was found to be comparable to that WTM w.r.t. the choice of LF when parameter AuC was  
17 considered. Stronger differences were observed when one considers the second criterion (TPR at fixed  
18 FPR = 0.05). Interestingly, the performance of WTM was found to dramatically decrease when the LF  
19 band included very low frequencies (lowest performance obtained for LF = ]0, 32] Hz for human and  
20 animal data). Finally, both methods exhibited best results for ]32-64] Hz and ]32-128] Hz bands with  
21 an AuC almost equal to 0.99 (see grey boxes in tables 3 and 4). WTM had similar performance than  
22 FTM in term of AuC but slightly lower performance (0.94 vs. 0.96 for both human and animal data) in  
23 term of TPR for a FPR fixed at 0.05. This result could be explained by a detailed analysis of the ROC  
24 curves which showed that, for FTM, the TPR increased in a steep manner at low FPR (2 to 5 %) but  
25 reached the value of 1 for higher values. These results led us to choose the band ]32, 128] Hz as the  
26 LF band to estimate the occurrence times of FRs (see eq. 2 and eq. 3) in simulated and real signals, as  
27 reported hereafter.

1

Data	Method	Class	Closest Gaussian distribution		Kolmogorov test (Normal law)	
			Mean	Variance	Significance level	Result
Human	FTM	FR	0.06897	0.00083	0.05	Positive
		IES	0.00707	0.00010	0.05	Positive
	WTM	FR	0.04047	0.00009	0.05	Positive
		IES	0.01048	0.00005	0.05	Positive
Animal	FTM	FR	0.08900	0.00225	0.05	Positive
		IES	0.00638	0.00010	0.05	Positive
	WTM	FR	0.09333	0.00058	0.05	Positive
		IES	0.02374	0.00021	0.05	Positive

2

3 **Table 2:** Estimated mean and variance of the FTM and WTM criteria, and results of the Kolmogorov test.

4

		[0,512]	[0,256]	[0,128]	[0,64]	[0,32]	[128,256]	[64,128]	[32,64]	[32,128]
<b>FTM</b>	<i>AuC</i>	0.955	0.955	0.955	0.952	0.945	0.883	0.973	0.983	0.982
	<i>TPR for a FPR value of 0.05</i>	0.503	0.503	0.503	0.483	0.440	0.238	0.822	0.965	0.968
<b>WTM</b>	<i>AuC</i>	0.912	0.912	0.912	0.909	0.918	0.960	0.975	0.986	0.986
	<i>TPR for a FPR value of 0.05</i>	0.355	0.355	0.355	0.355	0.276	0.766	0.897	0.945	0.943

5

6 **Table 3:** Human data (TLE, hippocampus). Influence of the choice of the LF band in FTM and WTM. Both  
7 methods show best performance for the 32-128 Hz and 32-64 Hz bands. Gray boxes indicate best performance.  
8 See glossary for abbreviations.

9

10 *Threshold analysis of FTM and WTM*11 We give in table 2 the mean and variance of FTM and WTM criteria as well as the result of the  
12 Kolmogorov test. We divided results between human and animal data. We found that all the  
13 distributions were Gaussian and that the mean value of FRs was always greater than the mean values  
14 of IES. Moreover, these mean values of the criteria do not differ so much from human to animal data  
15 (0.07 and 0.09 for FTM, and 0.04 and 0.09 for WTM). From these estimated Gaussian distributions

1 the optimal threshold and the related good detection rate as a function of the FR rate are given in  
 2 figure 5. We found that the optimal threshold did not vary significantly for FR rate ranged from 0.1 to  
 3 0.9. The related good classification rates was high ( $>0.93$ ) when the optimal threshold was computed  
 4 from a known FR rate. This good classification rates remained high ( $>0.9$ ) when the optimal threshold  
 5 was computed from FR rate arbitrarily set to 0.5.

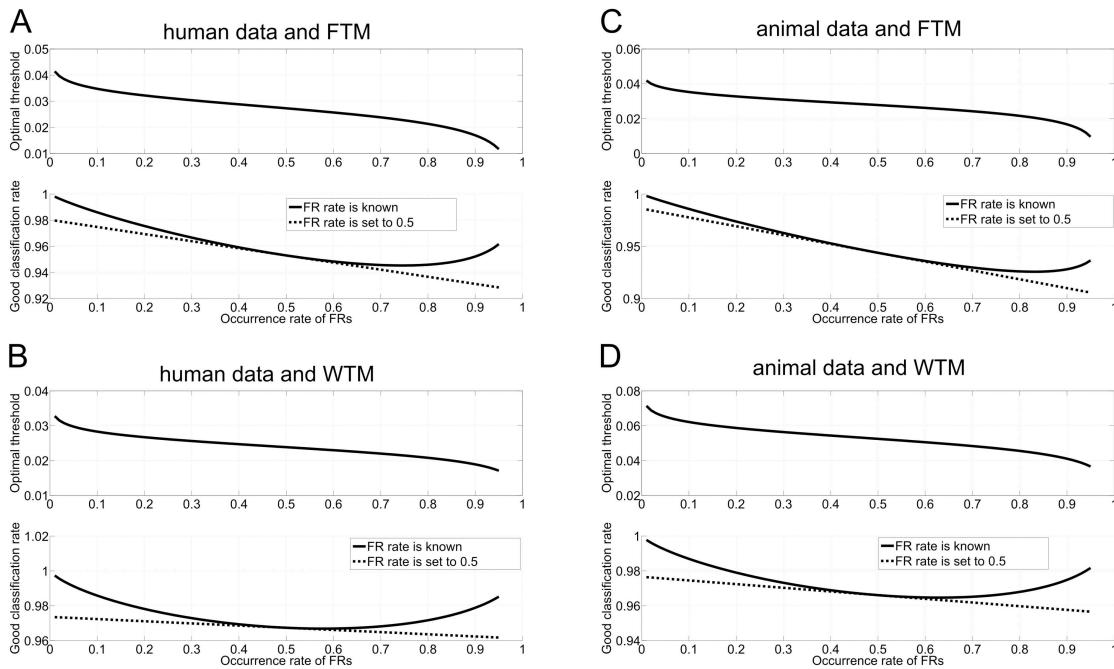
6

		]0,512]	]0,256]	]0,128]	]0,64]	]0,32]	]128,256]	]64,128]	]32,64]	]32,128]
<b>FTM</b>	<i>AuC</i>	0.835	0.835	0.836	0.832	0.818	0.956	0.987	0.990	0.991
	<i>TPR for a FPR value of 0.05</i>	0.588	0.592	0.592	0.579	0.542	0.693	0.920	0.935	0.964
<b>WTM</b>	<i>AuC</i>	0.896	0.896	0.896	0.898	0.899	0.988	0.990	0.994	0.995
	<i>TPR for a FPR value of 0.05</i>	0.788	0.788	0.791	0.798	0.740	0.939	0.977	0.941	0.945

7

8 **Table 4:** Animal data (mouse, kainate model of TLE, hippocampus). Influence of the choice of the LF band in  
 9 FTM and WTM. Both methods show best performance for the 32-128 Hz and 32-64 Hz bands. Gray boxes  
 10 indicate best performance. See glossary for abbreviations.

11



12

13 **Figure 5:** Optimal threshold and good classification rate of the methods as a function of the occurrence rate of  
 14 fast ripples. For each graph, on top is the optimal threshold as a function the fast ripple rate. On the bottom is the

1 good classification rate associated with this optimal threshold (solid line), and the good classification associated  
 2 with a threshold determined as if the fast ripple rate was equal to 0.5 (dashed line). A. Human data and FTM  
 3 method. B. Human data and WTM. C. Animal data and FTM. D. Animal data and WTM.  
 4 product.

5

FRBR	Criterion	HPFM	FTM	WTM
<b>No BKG</b>	<i>AuC</i>	0.668	0.984	0.993
	<i>TPR for FPR = .05</i>	0.147	0.970	0.935
<b>15 dB</b>	<i>AuC</i>	0.668	0.984	0.992
	<i>TPR for FPR = .05</i>	0.147	0.970	0.930
<b>5 dB</b>	<i>AuC</i>	0.627	0.852	0.891
	<i>TPR for FPR = .05</i>	0.124	0.324	0.467
<b>-5 dB</b>	<i>AuC</i>	0.501	0.679	0.889
	<i>TPR for FPR = .05</i>	0.049	0.129	0.458

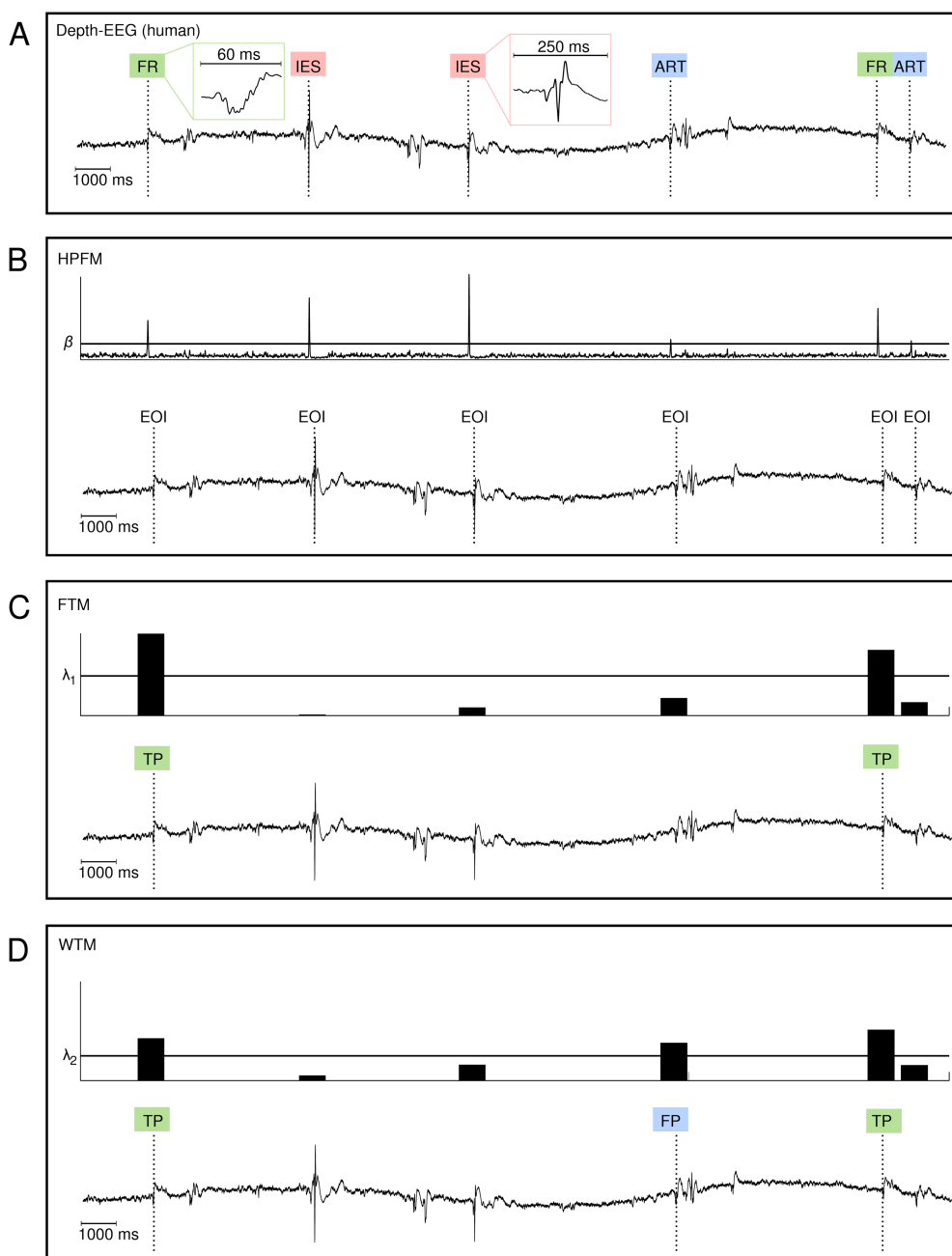
6

7 **Table 5:** Influence of the FRBR on the performance of HPFM, FTM and WTM. HPFM exhibits low AuC for all  
 8 values of FRBR indicating a conceptual inability of the method for distinguishing FRs from IES. For FTM and  
 9 WTM, the AuC decreases with the FRBR. WTM is more robust for low FRBR. Gray boxes indicate best  
 10 performance. See glossary for abbreviation.

11

12 *Simulated signals.* We compared the performance of the three methods (HPFM, FTM and WTM)  
 13 using signals simulated as described in section 2.3.3. The interesting aspect of such simulations is that  
 14 the level of background activity, characterized by the FRBR, could be varied. Results are given in  
 15 Table 5. First, they revealed that the HPFM exhibited very low performance whatever the level of  
 16 background activity relative to that of EOIs to be detected. This means that a simple high-pass filtering  
 17 procedure could not discriminate FRs from IESs. In other word, this result showed that the signal  
 18 energy beyond 256 Hz could not be used alone as a criterion to detect FRs. Second, results also  
 19 showed that FTM and WTM exhibited comparable results for a FRBR equal to 15 dB (which  
 20 corresponded to the value estimated from real data): in both cases, the AuC was found to be high  
 21 (>0.98) as was TPR (> 0.93) for a fixed FPR equal to 0.05. As expected, when the amplitude of EOIs  
 22 to be detected became low w.r.t. the amplitude of background activity (FRBR = 5 dB and FRBR = -5

1 dB), the performance of both methods decreased. Interestingly, WTM showed higher robustness w.r.t.  
 2 this parameter (AuC = 0.889 and TPR = 0.458) compared to FTM (AuC = 0.679 and TPR = 0.129) in  
 3 a situation where EOIs were (almost) impossible to detect visually (FRBR = -5dB). This result can be  
 4 explained by the use of a mother wavelet in WTM which shape is close to that of actual FRs in the  
 5 256-512Hz band. This “shape fitting” allows for changes that can still be detected in the convolution



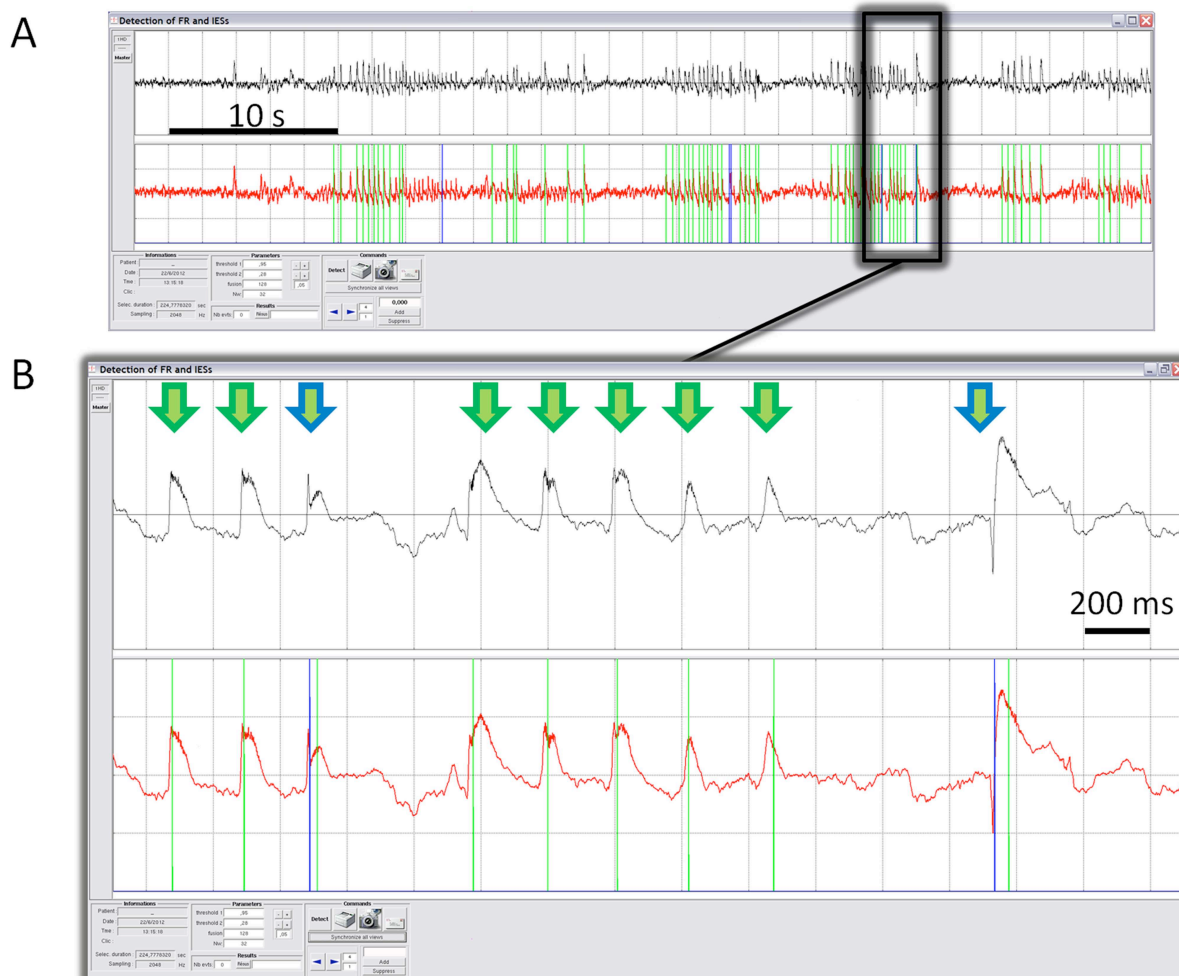
6  
 7 **Figure 6:** Behavior of proposed methods on real human data (A). The short-time energy in the 256-512 Hz band  
 8 (B) shows peaks at occurrence times of EOIs, which can be either FRs, IESs or artifacts. (C) Fourier Transform  
 9 based method. Top: ratio between energies in the 256-512 Hz band and in the 32-128 Hz band. Bottom: detection

1 results after thresholding. (D) Wavelet Transform based method. Top: ratio between energies in the 256-512 Hz  
 2 band and in the 32-128 Hz band. Bottom: detection results after thresholding. For both methods, the two  
 3 FRs are properly detected (true positives, TP). Note that some false positives (FP) can always be present (as for  
 4 WTM in this example). See glossary for abbreviations.

5  
 6 *Real signals.* Figure 6 provides a typical example showing the behaviour of the studied methods  
 7 (HPFM, FTM and WTM). A 20 second segment of human data (Figure 6A, see also section 2.1.1) was  
 8 used for this purpose. The first stage of the detection procedure is illustrated in figure 6B where the  
 9 signal energy in the 256-512 Hz band is plotted as a function of time. Very clear and sharp spikes  
 10 appeared at the time instants where EOIs (defined as events exhibiting energy in the HF band) were  
 11 present in the depth-EEG signal. This segment was chosen for the presence of three types of EOIs (see  
 12 FR, IES and ART labels in Figure 6A). In the first stage of the detection procedure, HPFM makes use  
 13 of a threshold  $\beta = 1.5$  (corresponding to 0.98 percentile) to extract EOIs (marked on the signal by a  
 14 vertical line). For the second stage, the behaviour of FTM is displayed in Figure 6C where we  
 15 represented the criterion value (i.e.  $E_{\Delta HF/LF}^{FTM}(p)$ ) for each EOI detected by HPFM at the first stage.  
 16 Detection results were obtained for a threshold value equal to  $\lambda_1 = 0.030$ . In this example, FTM  
 17 detected both FRs (marked as True Positive (TP)) and did not exhibit false detection (FP) since the  
 18 two IESs and the two artifacts were rejected. Finally, results obtained with WTM are displayed in  
 19 figure 5C. In this example, using a threshold value equal to  $\lambda_2 = 0.025$ , the method could detect both  
 20 FRs (as wanted) but also exhibited a false positive.

21 *Quasi-simultaneous FRs and IESs.* We implemented both methods in a user-friendly software that  
 22 allows for direct visual assessment of the detector performance on real data. The graphical user  
 23 interface is illustrated in figure 7A. It includes two plots showing the raw signal (upper plot, black  
 24 color) and the same signal (lower plot, red color) on top of which automatically detected EOIs are  
 25 marked by vertical bars (FRs: green color, IES: blue color). This GUI offers strong magnification on  
 26 EOIs for careful visual inspection of detection results, as illustrated in figure 7B. In this example, one  
 27 can observe the behaviour of the proposed detection method (here FTM) in the case where both the  
 28 IES and the FR occur quasi-simultaneously (a few tens of ms delay). Interestingly, the detector is able

1 to automatically mark both events when the duration  $N$  of the sliding Hanning window used in the first  
 2 stage of the detection procedure is short enough (32 ms in this case).



3  
 4 **Figure 7:** Implementation of the proposed detector (FTM) in a user-friendly software specifically designed to  
 5 directly inspect detection results. (A) The user selected in the EEG reviewing software (not shown) a segment of  
 6 about 224 s of data (upper plot). Detection results appear directly on the signal (lower plot, red trace) as green  
 7 bars (FRs) or blue bars (IESs). (B) A zoom on a 3 s segment of signal (upper plot). In this segment, FRs (green  
 8 arrows) and mixed IESs/FRs (bleu/green arrows) occur. As seen in detection results (lower plot), all FRs are  
 9 detected. In addition, two bars (blue and green) are automatically positioned by the detector in the presence of  
 10 quasi-simultaneous IESs and FRs.

## 11 **4. Discussion and perspectives**

12 The detection of transient events in EEG signals has long been a topic of large interest in clinical  
 13 neurophysiology. This problem has been - and is still - considered as a difficult problem in signal  
 14 processing. During the past decades, many methods were proposed to automatically detect interictal

1 epileptic spikes (IESs), starting from pioneering works of Gotman (Gotman and Gloor, 1976).  
2 Proposed algorithms were based on Fourier or wavelet transforms, on mimetic and rule-based  
3 approaches, on neural networks, on adaptive filtering (template matching), on principal or independent  
4 component analysis. Readers may refer to (Gotman, 1999) and to (Fleureau et al., 2011a; Tzallas et al.,  
5 2006) for partial reviews.

6 Recently, fast ripples (FRs) have attracted a lot of attention since they could constitute an interictal  
7 electrophysiological marker for epilepsy (Engel et al., 2009; Jefferys et al., 2012). Indeed, FRs might  
8 prove more specific than IESs with respect to the underlying epileptogenicity (Demont-Guignard et  
9 al., 2012) and might be more specifically generated in brain structures involved at the onset of seizures  
10 (Zijlmans et al., 2009). In this context, the reliable detection of fast ripples (FRs) can provide  
11 additional and quantified arguments to epileptologists to assess the epileptogenic nature of some brain  
12 structures explored with intracranial electrodes.

13 Conversely to IESs, very few methods have been proposed so far to automatically and specifically  
14 detect FRs in EEG signals. This is the issue we addressed in this study. To proceed, we proposed a  
15 novel detection procedure based on two stages (global detection of EOIs and local classification). The  
16 evaluation methodology was based on the simulation of long-duration depth-EEG signals and on ROC  
17 curves. Finally, tests were performed on real data recorded either in a patient with TLE or in an animal  
18 model of TLE.

19 The main findings of this study are summarized hereafter, first from a methodological viewpoint, and  
20 then from a clinical viewpoint.

21 *The use of simulated signals.* We decided to start from realistic simulations of depth-EEG signals.  
22 Simulated signals were obtained from the insertion of real EOIs (namely FRs and IESs) into  
23 background EEG activity generated from a neural mass model published elsewhere (Wendling et al.,  
24 2002). This approach provided a “ground truth” on both the occurrence time and the type of EOIs that  
25 is crucial in the objective assessment of any detection procedure. In addition, this approach also  
26 allowed us to test an important factor that was not tested in previous reports (Gardner et al., 2007;  
27 Staba et al., 2002; Zelmann et al., 2012): the detection robustness when the amplitude of background  
28 EEG becomes predominant w.r.t. the amplitude of EOIs to be detected.

1 *A two-stage detection procedure.* The basic principle of the proposed method is to first perform a  
2 global detection of EOIs (defined as transient events leading to an increase of signal energy within the  
3 256-512 Hz frequency band) and then perform a local analysis to assign each EOI to a specific class  
4 (FR vs. IES or artifacts). We found that the combination of the two stages could bring an appropriate  
5 solution to the problem of automatically identifying FRs in depth-EEG signals. The first stage consists  
6 of a classical high-pass filtering (cut-off frequency: 256 Hz). It could be achieved using any filter  
7 (either infinite or finite impulse response) as we found that detection results were independent from  
8 the filter design procedure. It is worth mentioning that this first stage is also inspired from a current  
9 practice in EEG analysis. Indeed, high-pass filtering of EEG signals (available on most EEG  
10 reviewing softwares) is classically used by epileptologists to get rid of the background activity and to  
11 better reveal some signal oscillations occurring in the frequency band of interest, typically the high-  
12 frequency band. However, it should be also reminded that both FRs and sharp transients (like IESs)  
13 both lead to such oscillations in the 250-500 Hz (“fast ripples” vs. “false ripples”), as demonstrated in  
14 (Benar et al., 2010). In our method, the first stage is complemented by a second stage which makes use  
15 of the energy distribution (in the frequency domain) of the signal to classify EOIs. Two variants were  
16 proposed for this second stage, either based on the Fourier (FT) or the Wavelet (WT) Transform.  
17 These two transforms were used to compute a crucial parameter for distinguishing FRs from other  
18 EOIs: the energy ratio between high frequency (HF, 250-500 Hz) and low frequency (LF) bands. The  
19 choice for the LF band is discussed below (see § *Parameters to be adjusted*). A comparable procedure  
20 was proposed in (Blanco et al., 2010) where a data mining procedure is used on candidate HFO events  
21 detected by a high-pass filtering procedure (Staba et al., 2002). This unsupervised data mining  
22 provides several classes that allow for the discrimination of different kinds of HFOs and artifacts.  
23 While the method is very effective to achieve this goal, it looks like it requires more effort for  
24 implementation compared to our method and is probably more demanding in term of computing time.  
25 In addition, although unsupervised, training sets are necessary which is not the case in our method.  
26 Besides, the issue of IES and IES superimposed with FRs was not addressed by the authors. In this  
27 respect, our intent was different as we specifically addressed the “false ripples” issue due to sharp

1 transients (IES) (Benar et al., 2010). In addition, our method is conceptually simple. In practice, it is  
2 easy to implement and use.

3 *Specificity and sensitivity.* The method was found to show slightly improved performance when the  
4 WT is used for the second stage. In all studied situations, results showed that the use of the FT or the  
5 WT for the second stage lead to a much higher performance compared to the use of a simple high-pass  
6 filter. Using the WT, the method could achieve the detection of FRs with sensitivity greater to 0.93  
7 when the specificity was set to 0.95. In other words, in a situation where 95% of detected EOIs are  
8 actually FRs, only 7% of these EOIs are missed (either undetected or wrongly labeled) by the  
9 proposed method. As expected, we also found that the method performance depends on the amplitude  
10 of FRs respective to the level of background activity. As the “fast ripple to background” ratio (FRBR)  
11 decreased, the method sensitivity rapidly dropped when high specificity was maintained. However, it  
12 should be noted that the poorer performance (45.8% sensitivity) was obtained in a situation where the  
13 FRBR was so low (- 5 dB) that FRs became undetectable by visual inspection.

14 *Parameters to be adjusted.* An interesting feature of the proposed method is that the number of  
15 parameters to be adjusted is rather limited. For the first stage, any band pass filter (250-600 Hz) can be  
16 used to compute the signal energy in the FR frequency band and then to obtain EOIs by thresholding  
17 (parameter  $\beta$ ). For the purpose of this study, we used a 4<sup>th</sup> order Butterworth filter with cut-off  
18 frequencies equal to 256 Hz and 512 Hz to have a correspondence with the FTM and the WTM. An  
19 IIR implementation (recursive filter) was preferred for its rapidity. Parameter  $\beta$  can be easily adjusted  
20 from the empirical histogram of the filtered signal energy values (see §2.2.2). For the second stage of  
21 the detection procedure, the essential parameter to distinguish FRs from IESs was found to be the  
22 energy ratio between high and low frequency bands (HF and LF, respectively). The HF band must be  
23 adjusted to best match the frequency band of FRs (typically, 250-600 Hz). In this study, we used a HF  
24 band ranging from 256 Hz to 512 Hz, constrained by the dyadic discrete wavelet transform. We let the  
25 LF band as a free parameter and obtained the best results (in term of separation of FRs from IESs) for  
26 a LF band equal to [32-128 Hz] which coincided with the gamma frequency band on the EEG. This  
27 result also indicates that our method is likely to not be affected by slow waves (typically in the delta  
28 frequency band) which can be present in EEG signals during sleep, in particular.

1 Finally, for the WTM, the mother wavelet and the number of levels must also be adjusted. We tested  
2 several configurations (data not shown). Best results were obtained for a Daubechies 4 wavelet  
3 decomposition on eight or nine levels depending on the sampling frequency (1024 and 2048 Hz,  
4 respectively). The classification of FRs and IESs is done by thresholding the energy ratio between  
5 high and low frequency bands. Interestingly, one can notice that these values do not differ so much  
6 from one recording to another (same order of magnitude). This result indicates that the energy  
7 distribution in proposed sub-bands (gamma and FR) is robust with respect to the type of recording  
8 (performed in humans and in mice) and suggests that the algorithm can be used in some other  
9 situations (like other experimental models of epilepsy) characterized by the occurrence of HFOs in the  
10 FR frequency band (HF subband).

11 *Potential clinical value.* Both methods are relatively easy to implement. Besides the performance  
12 study (in term of recognition of FRs and IESs), we could also analyse more difficult situations where  
13 genuine FRs occur quasi-simultaneously with, or are part of, IESs. Indeed, the co-occurrence of spikes  
14 and fast ripples (denoting different pathological condition of underlying neuronal systems) can be  
15 encountered and consequently is also relevant to detect. . Interestingly, for appropriate setting of the  
16 time window used in the first stage, and given that both types of events do not occur strictly at the  
17 same time, our method can still separate them. More generally, in most of epilepsy surgery units,  
18 recordings are performed in patients candidate to surgery using long-term video-EEG monitoring (8-  
19 24 hours a day, 5-10 days). Huge data sets are generated by the acquisition systems since signals are  
20 generally recorded on 128 to 256 channels at 1 kHz. We think that the proposed detection method can  
21 dramatically decrease the workload in assessing the presence of FRs in these intracranial EEGs. In  
22 addition, it may allow for systematic identification of FRs during interictal periods which represent  
23 large amounts of data compared to seizure episodes. To us, it is clear that the therapeutic strategy  
24 cannot depend only of the presence/absence of high frequency oscillations (HFOs) in explored brain  
25 structures. However, the objective quantification of HFOs over interictal periods can efficiently  
26 complement the classical often qualitative way of analyzing depth-EEG data recorded in patients with  
27 drug-resistant epilepsy.

1 *Perspectives*. The online implementation of the proposed method is a topic of interest for future work.  
 2 In addition, some other time-frequency methods (empirical mode decomposition (Fleureau et al.,  
 3 2011a; Fleureau et al., 2011b) and matching pursuit (Jmail et al., 2011; Mallat and Zhang, 1993) in  
 4 particular) could also be tested in the second stage of the detection procedure to check whether the  
 5 overall performance could still be increased. Finally, these detection methods (based on time-  
 6 frequency features of the signal) will also be compared with that recently proposed methods by Blanco  
 7 et al. (Blanco et al., 2010) and Zelmann and collaborators (Zelmann et al., 2012), although not  
 8 designed to specifically detect FRs but HFOs in a more general way. This comparative study should  
 9 be doable since time-frequency based methods can be adapted quite straightforwardly to the detection  
 10 of ripples (128-256 Hz) in addition to fast ripples. Such a comparison will be performed through the  
 11 use of different performance metrics as suggested by Casson et al. (Casson et al., 2009).

## 12 **Acknowledgement**

13 This work was supported by “Region Bretagne” (CRITT Santé Bretagne, « RIPPLE » project, 2012).

## 14 **Appendix**

### 15 A. Optimal threshold

16 For an Event Of Interest (EOI), we have two hypothesis.  $\mathbf{H}_1$ : the EOI is a Fast Ripple (FR) and  $\mathbf{H}_0$ : the  
 17 EOI is not a FR. Let  $R$  be the high frequency to low frequency ratio given in section 2.2 and  $\lambda$  the  
 18 threshold that discriminates EOIs that are FR from the ones that are not. To be optimal, this threshold  
 19 has to maximize the probability to take the good decision, i.e. to detect a FR when the EOI is actually  
 20 an FR and to not detect an FR when the EOI is not an FR. This probability, also called one minus  
 21 classification error rate, is given by  $P_{ne} = P(ne \cap H_1) + P(ne \cap H_0)$  where  $ne$  stands for “no  
 22 error”. This can be written with conditional probabilities as:

$$23 \quad P_{ne} = P(H_1) P(ne / H_1) + P(H_0) P(ne / H_0)$$

$$24 \quad P_{ne} = P(H_1) P(R \geq \lambda / H_1) + P(H_0) P(R < \lambda / H_0)$$

$$25 \quad P_{ne} = P(H_1) P(1 - P(R < \lambda / H_1)) + P(H_0) P(R < \lambda / H_0)$$

1 Thus we have to maximize  $P_{ne}$  with respect to  $\lambda$ , i.e. to find the roots of the derivative of  $P_{ne}$  with  
 2 respect to  $\lambda$ . The derivative is given by:

$$3 \quad \frac{dP_{ne}}{d\lambda} = -P(H_1) p_R(\lambda/H_1) + P(H_0) p_R(\lambda/H_0)$$

4 where  $p_R(\lambda/H)$  is the conditional probability density function of  $R$  given  $H$ . Thus we have:

$$5 \quad \frac{p_R(\lambda/H_1)}{p_R(\lambda/H_0)} = \frac{P(H_0)}{P(H_1)}$$

6 Assuming that probability density functions are Gaussian, then we have:

$$7 \quad p_R(\lambda/H_1) = \frac{1}{\sigma_1 \sqrt{2\pi}} e^{-\frac{(\lambda-m_1)^2}{2\sigma_1^2}}$$

$$8 \quad p_R(\lambda/H_0) = \frac{1}{\sigma_0 \sqrt{2\pi}} e^{-\frac{(\lambda-m_0)^2}{2\sigma_0^2}}$$

9 where  $m$  is the mean and  $\sigma$  the standard deviation, and

$$10 \quad \frac{p_R(\lambda/H_1)}{p_R(\lambda/H_0)} = \frac{\sigma_0}{\sigma_1} e^{\frac{(\lambda-m_0)^2}{2\sigma_0^2} - \frac{(\lambda-m_1)^2}{2\sigma_1^2}}$$

11 Consequently we have to solve the following equation in order to find the optimal threshold:

$$12 \quad \frac{(\lambda-m_0)^2}{\sigma_0^2} - \frac{(\lambda-m_1)^2}{\sigma_1^2} - 2 \ln \frac{P(H_0)\sigma_1}{P(H_1)\sigma_0} = 0$$

13 Thus the optimal  $\lambda$ , denoted by  $\lambda_{opt}$  is one of the two roots of a second order polynomial function in  
 14 which the coefficients are known if  $m_0, m_1, \sigma_0, \sigma_1, P(H_0)$  and  $P(H_1) = 1 - P(H_0)$  are known. In  
 15 practice, the root which maximizes  $P_{ne}$  has to be chosen. The corresponding rate of good classification  
 16 is given by:

$$17 \quad P_{ne}(\lambda_{opt}) = \frac{1}{2} P(H_1) \left( \operatorname{erfc} \left( \frac{\lambda_{opt} - m_1}{\sigma_1 \sqrt{2}} \right) \right) + \frac{1}{2} (1 - P(H_1)) \left( \operatorname{erfc} \left( -\frac{\lambda_{opt} - m_0}{\sigma_0 \sqrt{2}} \right) \right)$$

18 where  $\operatorname{erfc}$  is the complementary error function given by  $\operatorname{erfc}(x) = \frac{2}{\sqrt{\pi}} \int_x^\infty e^{-t^2} dt$ .

1

2 **References**

- 3 Baker SN, Curio G, Lemon RN. EEG oscillations at 600 Hz are macroscopic markers for cortical  
4 spike bursts. *J Physiol*, 2003; 550: 529-34.
- 5 Bartolomei F, Guye M, Gavaret M, Regis J, Wendling F, Raybaud C, Chauvel P. [The presurgical  
6 evaluation of epilepsies]. *Rev Neurol (Paris)*, 2002; 158: 4S55-64.
- 7 Benar CG, Chauviere L, Bartolomei F, Wendling F. Pitfalls of high-pass filtering for detecting  
8 epileptic oscillations: a technical note on "false" ripples. *Clin Neurophysiol*, 2010; 121: 301-10.
- 9 Blanco JA, Stead M, Krieger A, Viventi J, Marsh WR, Lee KH, Worrell GA, Litt B. Unsupervised  
10 classification of high-frequency oscillations in human neocortical epilepsy and control patients. *J*  
11 *Neurophysiol*, 2010; 104: 2900-12.
- 12 Bouilleret V, Loup F, Kiener T, Marescaux C, Fritschy JM. Early loss of interneurons and delayed  
13 subunit-specific changes in GABA(A)-receptor expression in a mouse model of mesial temporal lobe  
14 epilepsy. *Hippocampus*, 2000; 10: 305-24.
- 15 Bragin A, Engel J, Jr., Wilson CL, Fried I, Buzsaki G. High-frequency oscillations in human brain.  
16 *Hippocampus*, 1999a; 9: 137-42.
- 17 Bragin A, Engel J, Jr., Wilson CL, Vizing E, Mathern GW. Electrophysiologic analysis of a chronic  
18 seizure model after unilateral hippocampal KA injection. *Epilepsia*, 1999b; 40: 1210-21.
- 19 Bragin A, Wilson CL, Staba RJ, Reddick M, Fried I, Engel J, Jr. Interictal high-frequency oscillations  
20 (80-500 Hz) in the human epileptic brain: entorhinal cortex. *Ann Neurol*, 2002; 52: 407-15.
- 21 Buzsaki G, Lopes da Silva F. High frequency oscillations in the intact brain. *Prog Neurobiol*, 2012;  
22 98: 241-9.
- 23 Crepon B, Navarro V, Hasboun D, Clemenceau S, Martinerie J, Baulac M, Adam C, Le Van Quyen  
24 M. Mapping interictal oscillations greater than 200 Hz recorded with intracranial macroelectrodes in  
25 human epilepsy. *Brain*, 2010; 133: 33-45.
- 26 Demont-Guignard S, Benquet P, Gerber U, Biraben A, Martin B, Wendling F. Distinct  
27 hyperexcitability mechanisms underlie fast ripples and epileptic spikes. *Ann Neurol*, 2012; 71: 342-52.
- 28 Engel J, Jr., Bragin A, Staba R, Mody I. High-frequency oscillations: what is normal and what is not?  
29 *Epilepsia*, 2009; 50: 598-604.
- 30 Fleureau J, Kachenoura A, Albera L, Nunes J, Senhadji L. Multivariate empirical mode decomposition  
31 and application to multichannel filtering. *Elsevier Signal Processing*, 2011a; 91: 2783-92.
- 32 Fleureau J, Nunes J, Kachenoura A, Albera L, Senhadji L. Turning Tangent Empirical Mode  
33 Decomposition: a unified framework for mono- and multivariate signals. *IEEE Transactions On Signal*  
34 *Processing*, 2011b; 59: 1309-16.
- 35 Gardner AB, Worrell GA, Marsh E, Dlugos D, Litt B. Human and automated detection of high-  
36 frequency oscillations in clinical intracranial EEG recordings. *Clin Neurophysiol*, 2007; 118: 1134-43.
- 37 Gotman J. Automatic detection of seizures and spikes. *J Clin Neurophysiol*, 1999; 16: 130-40.
- 38 Gotman J, Gloor P. Automatic recognition and quantification of interictal epileptic activity in the  
39 human scalp EEG. *Electroencephalogr Clin Neurophysiol*, 1976; 41: 513-29.
- 40 Jacobs J, LeVan P, Chander R, Hall J, Dubeau F, Gotman J. Interictal high-frequency oscillations (80-  
41 500 Hz) are an indicator of seizure onset areas independent of spikes in the human epileptic brain.  
42 *Epilepsia*, 2008; 49: 1893-907.
- 43 Jacobs J, Levan P, Chatillon CE, Olivier A, Dubeau F, Gotman J. High frequency oscillations in  
44 intracranial EEGs mark epileptogenicity rather than lesion type. *Brain*, 2009; 132: 1022-37.
- 45 Jefferys JG, de la Prida LM, Wendling F, Bragin A, Avoli M, Timofeev I, Lopes da Silva FH.  
46 Mechanisms of physiological and epileptic HFO generation. *Prog Neurobiol*, 2012.
- 47 Jmail N, Gavaret M, Wendling F, Kachouri A, Hamadi G, Badier JM, Benar CG. A comparison of  
48 methods for separation of transient and oscillatory signals in EEG. *J Neurosci Methods*, 2011; 199:  
49 273-89.
- 50 Mallat S, Zhang Z. Matching pursuit in a time-frequency dictionary. *IEEE Transactions on Signal*  
51 *Processing*, 1993; 41: 3397-415.
- 52 Papoulis A. *Probability, Random Variables and Stochastic Processes*. 3th edition, McGraw Hill, 1991.

- 1 Staba RJ, Wilson CL, Bragin A, Fried I, Engel J, Jr. Quantitative analysis of high-frequency  
2 oscillations (80-500 Hz) recorded in human epileptic hippocampus and entorhinal cortex. *J*  
3 *Neurophysiol*, 2002; 88: 1743-52.
- 4 Suzuki F, Junier MP, Guilhem D, Sorensen JC, Onteniente B. Morphogenetic effect of kainate on  
5 adult hippocampal neurons associated with a prolonged expression of brain-derived neurotrophic  
6 factor. *Neuroscience*, 1995; 64: 665-74.
- 7 Tzallas AT, Oikonomou VP, Fotiadis DI. Epileptic spike detection using a kalman filter based  
8 approach. *Conf Proc IEEE Eng Med Biol Soc*, 2006; 1: 501-4.
- 9 Wendling F, Bartolomei F, Bellanger JJ, Chauvel P. Epileptic fast activity can be explained by a  
10 model of impaired GABAergic dendritic inhibition. *Eur J Neurosci*, 2002; 15: 1499-508.
- 11 Wendling F, Hernandez A, Bellanger JJ, Chauvel P, Bartolomei F. Interictal to ictal transition in  
12 human temporal lobe epilepsy: insights from a computational model of intracerebral EEG. *J Clin*  
13 *Neurophysiol*, 2005; 22: 343-56.
- 14 Worrell G, Gotman J. High-frequency oscillations and other electrophysiological biomarkers of  
15 epilepsy: clinical studies. *Biomark Med*, 2011; 5: 557-66.
- 16 Worrell GA, Parish L, Cranstoun SD, Jonas R, Baltuch G, Litt B. High-frequency oscillations and  
17 seizure generation in neocortical epilepsy. *Brain*, 2004; 127: 1496-506.
- 18 Zelmann R, Mari F, Jacobs J, Zijlmans M, Dubeau F, Gotman J. A comparison between detectors of  
19 high frequency oscillations. *Clin Neurophysiol*, 2012; 123: 106-16.
- 20 Zijlmans M, Jacobs J, Zelmann R, Dubeau F, Gotman J. High-frequency oscillations mirror disease  
21 activity in patients with epilepsy. *Neurology*, 2009; 72: 979-86.
- 22
- 23